# Novel Framework for Registration of Pedobarographic Image Data

Francisco P. M. Oliveira[*], João Manuel R. S. Tavares[#]

[*]*Faculdade de Engenharia da Universidade do Porto (FEUP) / Instituto de Engenharia Mecânica e Gestão Industrial (INEGI), Rua Dr. Roberto Frias, 4200-465 Porto, Portugal*

[#]*Faculdade de Engenharia da Universidade do Porto (FEUP), Departamento de Engenharia Mecânica (DEMec) / Instituto de Engenharia Mecânica e Gestão Industrial (INEGI), Rua Dr. Roberto Frias, 4200-465 Porto, Portugal*

Corresponding Author:

Professor João Manuel R. S. Tavares

Phone: +351 225 081 487

Fax: +351 225 081 445

Email: tavares@fe.up.pt

url: www.fe.up.pt/~tavares

The total number of words of the manuscript, including entire text from title page to figure legends: ≅ 6400

The number of words of the abstract: 191

The number of figures: 4

The number of tables: 4

**Abstract**

This paper presents a framework to register plantar pressure images based on a hybrid registration approach, which first establishes an initial registration that is subsequently improved by the optimization of a selected image (dis)similarity measure. The initial registration has two different solutions: one based on image contour matching and the other on image cross-correlation. In the final registration, a multidimensional optimization algorithm is applied to one of the following (dis)similarity measures: the mean squared error (MSE), the mutual information (MI) and the exclusive or (XOR). The framework has been applied to intra and inter-subject registration. In the former, the framework has proven to be extremely accurate and fast (< 70 ms on a normal PC notebook), and obtained superior XOR and identical MSE values compared to the best values reported in previous studies. Regarding the inter-subject registration, by using rigid, similarity, affine projective and polynomial (up to the $4^{th}$ degree) transformations, the framework significantly optimized the image (dis)similarity measures. Thus, it is considered to be very accurate, fast and robust in terms of noise, as well as being extremely versatile, all of which are regarded as essential features for near-real-time applications.

***Keywords*** *Biomechanics, Plantar pressure data, Image registration, Optimization*

# 1. Introduction

Plantar pressure distribution provides significant information for researchers and specialists in the medical field as to the structure and function of the foot in addition to the general mechanics of human gait. It is, therefore, extremely helpful in the diagnosis of foot complaints, development of footwear [1, 2] and to obtain useful information for gait analysis [5, 6], to name just a few examples. Also plantar pressure distribution is capable of comparing the loads in the limb of injured and non-injured patients, pre- and post-traumatic injuries or operative states [19]. Furthermore, it is proficient in comparing patients and control groups and provides detailed information that is specific to each region of contact [19]. There are a number of different techniques to access the relevant pressure distribution, and, for the majority of these techniques, the pedobarographic data can be converted into a discrete rectangular array. Therefore, image processing and analytical techniques can be used directly in helping both researchers and medical specialists to obtain relevant information from the acquired digital data. Image registration methods, i.e., methods of optimally aligning homologous structures represented by images, which work accurately as far as pedobarographic data is concerned, are in great demand. For example, intra-subject registration is extremely valuable for researchers and specialists in the medical field to compare accurately the plantar pressure of a patient over time, pre- and post-traumatic injuries or operative states, or build a model that reveals the pressure distribution of a person's foot accurately. On the other hand, the inter-subject registration is essential to build foot databases, i.e. an atlas that can store foot data correctly aligned to a common referential system, that can compare a particular foot with feet previously studied, that can assist in the segmentation of feet into their main regions from plantar pressure images, and that can support automatic foot classification.

Besides the aforementioned advantages, pedobarographic image registration supports pixel-level statistics, which makes the acquisition of biomechanically-relevant information from plantar pressure images more effective than from the traditional regional techniques currently being used [14]. Thus, the fully automatic, accurate and fast methods for pedobarographic image registration are extremely useful to free researchers and medical specialists from tedious and

time-consuming tasks required by the traditional manual or semi-automatic registration solutions used nowadays.

Several studies on pedobarographic image registration have been carried out, such as: the use of principal axis transformations [7], modal matching [3, 17], principal axis combined with a search following the steepest descent gradient method [15], optimization based on genetic algorithms [16] and alignment based on the foot size and the foot progression angle [8], to name just a few. In [12] and [13] two conceptually different solutions are presented in order to register pedobarographic image data. The first is a feature-based method, based on the matching of the points of the contours obtained from the feet images that are to be registered. The latter is an intensity-based method which uses the intensity of image pixels to determine the geometric transformation that maximizes the cross-correlation (CC) between the images to be registered, which is computed in the frequency domain.

The main goal of this paper is to present a novel and fast framework for the registration of pedobarographic image data sets capable of using different (dis)similarity measures and geometric transformations (linear and curved) allowing for intra and inter-subject registration. In addition, the framework should be robust in terms of noise and able to register data sets acquired by distinct pedobarographic equipment efficiently, thereby overcoming the drawbacks of previous solutions. It should be emphasized that a high registration speed is very important for the framework since it is a crucial feature for its future acceptance and integration in real laboratory and clinical applications, especially for those near-real-time cases.

A second goal, also of great importance, is to compare the optimal geometric transformation obtained by inter-subject registration using various (dis)similarity measures. In [16], it was shown that in intra-subject registration, using rigid geometric transformation, the optimization of the conceptually very different (dis)similarity measures, mainly the mean squared error (MSE), mutual information (MI) and the exclusive or (XOR), leads to a similar geometric transformation. However, inter-subject registration is a completely different matter as each individual foot shape can be very distinctive as well as the foot pressure distributions. For instance, in some pedobarographic images only one toe is visible, while in others, all the toes are seen; and in some images, the region

between the forefront of the foot and the heel is represented whilst in others, it is not.

As far as registration experiments are concerned, in the intra-subject case, a rigid geometric transformation has been used. While in the inter-subject case, seven different geometric transformations were used: rigid, similarity, affine, projective and polynomials of the $2^{nd}$, $3^{rd}$ and $4^{th}$ degree.

Some current pedobarographic equipment, such as those based on light reflection techniques [17], can corrupt data acquired with noise that has a Gaussian distribution. The effect of this kind of noise on the proposed framework was studied and according to the results was shown to be robust.

Throughout this paper, we used the term "template image" to refer to the data set that is to remain unchanged and this was used as a reference and the term "source image" to refer to the data set that we aim to register, that is, align or transform. In addition, we employ the terms "contour-based" and "cross-correlation-based" to refer to the registration methods presented in [12] and [13], respectively.

This paper is organized as follows. The following section presents the novel framework that has been developed, the (dis)similarity measures, the data set used and the experiments. Section 3 gives the experimental results. Finally, in Section 4, the results are discussed and final conclusions are drawn.

# 2. Methods

This section presents all the fundamental principles of the methods integrated in the framework developed and explains the experimental settings which have been used.

## 2.1 The Framework

The framework developed to register pedobarographic image data uses a hybrid approach that can be divided in two distinct steps: 1) Estimation of an initial registration and 2) Establishment of the final registration through the optimization of a chosen (dis)similarly measure. The optimization step begins with the initial registration and then searches for the geometric transformation parameters that optimize the (dis)similarity measure adopted. Each geometric transformation parameter is considered as an independent variable in the multidimensional space,

and the (dis)similarity measure is the dependent variable that is to be optimized, i.e. minimized or maximized.

To establish the initial registration, two conceptually different solutions were used: the contour-based method [12] and the cross-correlation-based method [13].

To carry out the final registration based on the optimization of the image (dis)similarity measure adopted, an adaptation of the Powell's method [18] was employed.

The multidimensional optimization scheme based on Powell's method was tested by using two distinct solutions to carry out the line optimization with Powell's method: the robust golden section method, which is similar to the bisection method used to find a root of a one-dimensional function, and Brent's method, based on the parabolic interpolation in the neighborhood of the optimal value [18].

The novelties of the framework developed here, compared to our previous registration algorithms presented in [12] and [13], are the inclusion of an optimization procedure, which allows the optimization of the new image (dis)similarity measures, and the integration of non-similarity geometric transformations. The former solutions, the contour-based and cross-correlation-based methods proposed in [12] and [13], respectively, only allowed the computation of rigid or similarity geometric transformations, whereas the new framework allows the computation of affine, projective and polynomial up to the $4^{th}$ degree geometric transformations.

### *2.1.1 Contour-based registration method*

The contour-based registration method proposed in [12] can be subdivided into four main steps: I) Extract the external contours of the feet from the two images to be registered; II) Assemble the contour affinity matrix based on the following geometric features: curvature and distance [11]; III) Match the contour points by using an assignment algorithm based on the dynamic programming that preserves the order of the input points [10]; IV) Compute the parameters of the geometric transformation that minimize the distance between the matched points.

In the forth step of the contour-based method, besides the approach used in [12] to estimate the global geometric transformation that best aligns the contours, a standard approach based on the minimization of the sum of squared errors of the

Euclidean distances between the two sets of corresponding points, using the least-squares technique, has also been tested.

### *2.1.2 Cross-correlation-based registration method*

The cross-correlation-based registration method proposed in [13] is based on the maximization of the CC between the images, which is computed in the frequency domain by using the Fourier transform and Convolution theorem. The main steps are: I) Convert the two images to be registered to the frequency domain using the fast Fourier transform (FFT); II) Compute both spectrums and convert them to *log*-polar coordinates; III) Convert both *log*-polar spectrum images to the frequency domain using FFT; IV) Compute the cross-correlation matrix of the *log*-polar spectrums and determine the optimal shift of the *log*-polar spectrums based on the maximal value of that matrix (the translation along the $\log r$ axis permits one to determine the scaling, and the translation along the $\theta$ axis allows one to determine the rotation angle); V) Apply the scaling and rotation to the source image; VI) Convert the transformed image to the Fourier domain using FFT; VII) Compute the cross-correlation matrix of the images and determine the optimal translation between the template image and the rotated and scaled source image; VIII) Apply the computed rotation, scaling and shift to the original source image.

### *2.1.3 Powell's method*

Let $\vec{X} = (x_1, x_2, ..., x_n)$ be a vector that represents the independent variables and $f(\vec{X})$ the corresponding value of the dependent variable that should be minimized or, alternatively, maximized. Let $X_0 = (x0_1, x0_2, ..., x0_n)$ be an initial solution and $\mathbf{u}_i = \mathbf{e}_i$ ( $i = 1, ..., n$) the basis vector, which represents the original search directions resulting in $X_0 = x0_1\mathbf{u}_1 + x0_2\mathbf{u}_2 + ... + x0_n\mathbf{u}_n$. The ensuing estimation $X_1$ is generated by successively proceeding to a minimum or maximum of *f* along each of the *n* independent variables. This process generates a sequence of points $P_0, P_1, ..., P_n$, where $P_0 = X_0$. Next, based on the coordinates of $P_0$ and $P_n$, a new direction is computed and an optimization is performed along this new direction. Following this, one of the *n* previous

directions is removed and substituted by the new direction, and therefore the initial estimation is substituted by the new one. This process is repeated until the stop criterion is satisfied. For further explanations of this method, consult [18].

## 2.2 Geometric transformations

Seven distinct geometric transformations have been integrated in the framework and experimentally studied, namely: four "linear", i.e. rigid, similarity, affine and projective transformations, and three non-linear, modeled by using polynomial functions of the $2^{nd}$, $3^{rd}$ and $4^{th}$ degree. From a mathematical point of view, the rigid, similarity, affine and projective geometric transformations from $\Re^2$ to $\Re^2$ are not linear. However, for simplicity, we refer to them as "linear" since they always transform straight lines into straight lines in contrast with the polynomial functions of $2^{nd}$, $3^{rd}$ and $4^{th}$ that can transform straight lines into curves.

### *2.2.1 Rigid and similarity geometric transformations*

The process to determine the optimal rigid or similarity geometric transformation is relatively straightforward. The geometric transformation parameters computed by the registration method considered in the first step are used as entries into the optimization algorithm employed in the second step of the registration framework which is based on Powell's method. For a rigid geometric transformation, three independent parameters: angle and translations along the *x* and *y* axis, are taken into consideration. As for the similarity transformation, four independent parameters: scale, angle and translations along the *x* and *y* axis are used.

### *2.2.2 Affine, projective and polynomial geometric transformations*

In terms of the affine, projective and polynomial geometric transformations, the optimization method integrated in our framework initiates from the actual similarity geometric transformation, considering scale, angle and translations along the *x* and *y* axis, obtained by using the contour-based or the cross-correlation-based registration methods. By transforming the affine and the projective transformations into matrices and the coordinates of the image pixels into homogeneous coordinates, one has, respectively:

$$\begin{bmatrix} x' \\ y' \\ 1 \end{bmatrix} = \begin{bmatrix} a & b & e \\ c & d & f \\ 0 & 0 & 1 \end{bmatrix} \begin{bmatrix} x \\ y \\ 1 \end{bmatrix}, \tag{1}$$

$$\begin{bmatrix} x' \\ y' \\ w \end{bmatrix} = \begin{bmatrix} a & b & e \\ c & d & f \\ r & p & 1 \end{bmatrix} \begin{bmatrix} x \\ y \\ 1 \end{bmatrix}. \tag{2}$$

The first solution for parameters *a*, *b*, *c* and *d* are obtained from the initial scale and rotation, and the parameters *e* and *f* are obtained from the initial translation. For the projective transformation (Equation 2), parameters *r* and *p* define the projection point which is initially set to zero, and *w*, which is a dependent parameter, is used to normalize the pixel coordinates.

In the case of a polynomial geometric transformation, the process is similar to the previously described affine transformation process. However, it should be noted that the transformation matrix is different. For instance, for a polynomial transformation of the 2$^{nd}$ degree, the geometric transformation is obtained from:

$$\begin{bmatrix} x' \\ y' \\ 1 \end{bmatrix} = \begin{bmatrix} g & h & i & a & b & e \\ j & k & l & c & d & f \\ 0 & 0 & 0 & 0 & 0 & 1 \end{bmatrix} \begin{bmatrix} x^2 \\ xy \\ y^2 \\ x \\ y \\ 1 \end{bmatrix}. \tag{3}$$

To initiate the optimization process, the values for the parameters *a*, *b*, *c*, *d*, *e* and *f* are obtained from the previously determined similarity transformations, using the contour-based or the cross-correlation-based registration methods and the values of parameters *g*, *h*, *i*, *j*, *k*, and *l* are set to zero. For polynomial geometric transformations of a higher degree, the process is almost identical; the only difference being an increase in the number of parameters involved. Next, the Powell's optimization method is used to search for the values of all independent parameters that optimize the (dis)similarity measure.

In the case of the affine, projective and polynomial of the 2$^{nd}$, 3$^{rd}$ and 4$^{th}$ degree, there are 6, 8, 12, 20 and 30 independent parameters, respectively.

### 2.3 Similarity measures

The framework developed for hybrid registration permits the use of any intensity-based image (dis)similarity measure. In this study, we have applied four (dis)similarity measures previously used in pedobarographic image registration: XOR [16], two definitions of MSE, i.e. the standard and an additional definition considered in [16], and the MI [4, 21] based on the Shannon's entropy.

Let $I_0$ and $I_1$ be two discrete images of size $N \times M$ pixels and $bin(I_0)$ and $bin(I_1)$ the binarized versions of $I_0$ and $I_1$, respectively. Hence, the XOR between these images is computed as:

$$XOR = \frac{|bin(I_0) \oplus bin(I_1)|}{|bin(I_0)| + |bin(I_1)|} \times 100, \quad (4)$$

where $|.|$ is the cardinal function and $\oplus$ is the exclusive or operator. In the binarization process, the value 0 (zero) is attributed to all image pixels that have a pressure intensity equal to 0 (zero) and 1 (one) to all the other image pixels with a pressure intensity not equal to 0 (zero). Henceforth, this measure provides the percentage of non-overlapped pixels; thus, the lower the XOR values are the better the registrations are.

The MSE is well known and is represented as:

$$MSE = \frac{1}{N \times M} \sum_{i}^{N} \sum_{j}^{M} (I_0(i,j) - I_1(i,j))^2 . \quad (5)$$

Consequently, the lower the MSE value is, the better the input image data set register is. Additional, the slightly distinct MSE definition used in [16], which only considers the squared differences for pixels with a non-zero value, has also adopted in this paper and denoted as $MSE^*$.

MI was independently proposed by Collignon et al. [4] and by Viola and Wells [21] and is attained by:

$$MI = H(I_0) + H(I_1) - H(I_0, I_1), \quad (6)$$

where $H(I_k)$ is the Shannon's entropy of the pixels in image $I_k$ and

$$H(I_0, I_1) = -\sum_{j} \sum_{k} p(j,k) \log(p(j,k)) \quad (7)$$

is the joint entropy. For image registration purposes, higher MI values imply higher quality registrations. The MI was computed as in Mattes et al. [9] and using 32 bins in all experiments carried out.

### 2.4 Data

Data from previous studies [12, 13, 16] was used so as to have a direct comparison between the new framework and the former registration methods. The data set consisted of 30 pairs of peak pressure images acquired from 10 subjects, 3 image pairs per subject, at 500 Hz using a 0.5 m Footscan system (RSscan, Olen, Belgium). In order to compensate for the non-square sensor array spacing (5.08×7.62 $mm^2$/sensor, manufacturer specified), all images were vertically stretched by a factor of 1.5. Thus, each image pixel represented a squared region of 5.08×5.08 $mm^2$, and each image was specified by a rectangular grid of 45×63 pixels.

### 2.5 Registration assessment using experimental real images

Speed, $MSE^*$ and XOR accuracies attained by the framework were compared with the values obtained by using the global Min ($MSE^*$) and Min (XOR) methods based on evolutionary algorithms described in [16], the contour-based registration method described in [12] and the cross-correlation-based registration method presented in [13]. To allow for a suitable comparison, bilinear interpolation [20] to perform the geometric transformation of the image data sets and a rigid geometric transformation model were used, as in the indicated works.

### 2.6 Registration assessment using control images

Registration accuracy was also assessed by applying a known rigid geometric transformation to the set of 30 real image templates and subsequently measuring the residual error (RE) between the exact position expected for each pixel and the position estimated by the contour-based method, cross-correlation-based method and novel framework.

The reliability of the framework to Gaussian noise, which can be found in some real cases of pedobarographic data registration, was assessed by repeating the initial experiments on the original images after adding this kind of noise to them.

Throughout the optimization process, the XOR, MSE, MSE* and MI (dis)similarity measures were adopted. Additionally, the image transformations were carried out using bilinear and bicubic [20] interpolation throughout the entire transformation processes. Finally, the accuracy of the method was statistically evaluated by the two-sided *t* tests.

### 2.7 Registration assessment for inter-subject registration

To evaluate the accuracy of the framework for inter-subject registration, two experiments were conducted. In the first, the registration accuracy was assessed by applying a known warp geometric transformation to the set of 30 template images and subsequently measuring the RE and the image (dis)similarity measures. The second experiment began by randomly choosing one image from each of the 10 subjects (Sect. 2.4). Afterwards, each of these images was registered with the nine accompanying images. Hence, 45 different combinations were reached.

The registration tests were performed by using rigid, similarity, affine, projective and polynomial (up to the $4^{th}$ degree) geometric transformations. During the optimization process, XOR, MSE, MSE* and MI were used as the (dis)similarity measures.

In the two experiments, the accuracy of the methods under evaluation was statistically appraised by means of two-sided *t* tests.

### 2.8 Implementation

The proposed computational framework was fully implemented in $C^{++}$, using Microsoft Visual Studio 8, and our contour-based and cross-correlation-based registration methods, proposed in [12] and [13], respectively, were integrated into it.

The comparative tests were carried out using a standard PC notebook with an AMD Turion64 2.0 GHz microprocessor, 1.0 GB of RAM and running Microsoft Windows XP.

## 3. Results

As mentioned in Section 2.1, two types of line minimization were integrated with Powell's method: the golden section routine and the Brent's routine. Since the

results obtained by both routines were similar, only the Brent's routine results are presented below.

### 3.1 Registration accuracy assessment using experimental images

In addition to the results obtained using the proposed framework all reference results [12, 13, 16] are presented in Table 1.

(Insert Table 1 about here)

### 3.2 Registration accuracy assessment using control images

Table 2 shows the residual errors obtained by comparing the geometric transformation parameters estimated by the proposed registration framework, and the applied geometric transformation parameters. The values included in Table 2 are average values and were obtained with the following rigid geometric transformation control: rotation angle of 12º and shift equal to 2.50 pixels and -3.2 pixels. This geometric transformation control was chosen to simulate the maximal deformation observed from the experimental data set between trials of a subject. In the Table, the values associated to the (dis)similarity measures, XOR, MSE, $MSE^{*}$ and MI, were included. The results presented in Table 2 were obtained using bilinear interpolation in the resampling image transformations, similar results were also found using bicubic interpolation resampling.

(Insert Table 2 about here)

For the contour-based registration method, the geometric transformation was estimated using the least-squares technique after the points had been matched. The noise added to the images intensities had a Gaussian distribution with a zero mean (0 $N/cm^2$) and a standard deviation equal to 1.5 $N/cm^2$ (Figure 1). Pedobarographic data intensities are subject-dependent, and consequently, the signal to noise ratio (SNR) is subject-dependent too. For the pairs of 30 images with noise used, the SNR of pedobarographic image data varied between 1.4 and 3.5. The registration results obtained by the framework from the images with

noise (Table 2) were obtained without any preliminary image smoothing. It should be noted that the level of the Gaussian noise we added to the original images is significantly higher than the level that would usually be expected to be found in real applications demanding pedobarographic image registration.

(Insert Figure 1 about here)

### 3.3 Inter-subject registration accuracy

A comparison can be made between the residual errors and the image (dis)similarity measures shown in Table 3, considering a control warp geometric transformation (Figure 2). We defined the control geometric transformation as the sum of a projective transformation and a sinusoidal function:

$$\begin{bmatrix} x' \\ y' \\ w \end{bmatrix} = \begin{bmatrix} 1.1 & 0.2 & 0 \\ -0.3 & 1.0 & 1 \\ 10^{-4} & 0.002 & 1 \end{bmatrix} \begin{bmatrix} x \\ y \\ 1 \end{bmatrix} + \begin{bmatrix} 1.5\sin(0.3x) \\ 0 \\ 0 \end{bmatrix}. \qquad (8)$$

The projective transformation was chosen so that it includes a rotation, scale, shift and changes the ratio between different lengths of the associated foot, for instance, rearfoot and forefoot widths. On the other hand, the sinusoidal transformation was defined to introduce a curved distortion on the localization of the pixels. Afterwards, the different geometric transformation models and (dis)similarity measures used in the framework were applied to estimate the optimal geometric transformation.

(Insert Figure 2 about here)

Table 4 shows the average results obtained by the registration framework using XOR, MSE and MI as the image (dis)similarity measure for the inter-subject registration. The results obtained using both the cross-correlation-based and contour-based methods to compute the initial registrations were similar. As such, only the results obtained using the cross-correlation-based method to compute the initial guesses are included.

(Insert Table 4 about here)

Several examples of the deformation carried out on the source image to optimize the (dis)similarity measures are shown in Figure 3. In some non-linear registrations based on MSE optimization, the source image was very deformed, especially when bilinear interpolation was used. Figure 4 shows an example of this kind of deformation. However, when using bicubic interpolation, the geometric deformation was less than when using bilinear interpolation (Figure 4).

(Insert Figures 3 and 4 about here)

Based on a visual assessment, we concluded that in some cases of non-linear registration, i.e. polynomials of the $2^{nd}$, $3^{rd}$ and $4^{th}$ degree, when using the $MSE^{*}$, the geometric transformations obtained were unsuitable, despite the framework having optimized the $MSE^{*}$ considerably. Thus, no further tests were conducted using this dissimilarity measure.

# 4. Discussion

For the intra-subject registrations, the presented framework obtained $MSE^{*}$ values ($p<0.001$) superior to the contour-based and cross-correlation-based registration methods and an identical value to the best result indicated in [16]. However, compared to the method in [16], the framework required significantly less computational time. Also, when using the XOR as the dissimilarity measure and computing the initial registration with the contour-based method, the framework attained superior results to those reported in [13, 16] ($p<0.001$ and $p=0.015$, respectively) and a slight improvement relatively to the best result stated in [12]. The novel framework gave slightly different XOR values with each of the initial registration methods. This fact may be justified due to the behavior of XOR as a function: it is highly affected by image interpolation imperfections, in addition to not being continuous, and consequently two almost identical geometric transformations could produce very different XOR values and have local minimums. Thus, the convergence of the optimization algorithm to the global minimum cannot be guaranteed.

In terms of the intra-subject registration, the framework performed very fast (< 70 ms) for all tasks, that is, from the initial step (initiating the entire process with the hard disk data reading) to the final step (building of the last registered image), independently of the (dis)similarity measure and initial registration method used. In the tests carried out for the intra-subject registration using a known control geometric transformation, the results revealed an exceptionally high accuracy when MSE, MSE* and MI were optimized. After the optimization of the (dis)similarity measures, the residual errors diminish significantly ($p$<0.001) compared to the residual errors obtained using just the contour-based or the cross-correlation-based registration methods. The highest residual errors observed for the 30 image pairs were equal to $2.1\times10^{-5}$ pixel ($\cong10^{-4}$ mm) and 0.034 pixel ($\cong$0.17 mm) using both definitions of the MSE and the MI, respectively. As expected, by optimizing the XOR, the residual error was not as good: the maximum value observed was 0.28 pixel ($\cong$1.4 mm). The best residual errors were obtained by the framework considering the MSE and MSE* as dissimilarity measures ($p$<0.001).

For the images corrupted with Gaussian noise, the accuracy decreased slightly; however, it still remained very good. The optimization of the MSE and MSE* led to a significant improvement of the residual errors in comparison to the contour-based ($p$<0.001) and cross-correlation-based ($p$=0.04) registration methods. When compared with the contour-based method, the optimization of the MI produced inferior residual errors ($p$<0.001); however, some slight improvements were observed compared to the cross-correlation-based method ($p$=0.26). These findings show the reliability of the computational framework to data with noise (Table 2, Figure 1), specially when the MSE and MSE* are optimized.

As predictable, the results obtained for inter-subject registrations using a warping transformation (Table 3) show that the optimization algorithm successfully optimized the (dis)similarity measures. Nevertheless, for the case of the non-linear geometric transformation, the optimization of the (dis)similarity measure did not always lead to inferior residual errors. The best residual errors were obtained using the projective transformation, because the warping definition contains a strong projective component. The MSE* obtained, using a polynomial transformation of the 4th degree, was larger than the MSE* obtained with some of the geometric transformations of a lower degree of freedom. This fact shows that

the optimization algorithm converged for local minimums. On the other hand, the framework significantly ($p$<0.001) optimized the MSE as the degrees of freedom of the geometric transformation increased, which is an indication that the optimization algorithm converged to the global minimums or to the local minimums that are very close to them. Even though the MSE values improved significantly, the residual errors did not follow the same behavior, which is a somewhat expected when non-linear transformations are used.

The inter-subject registration results in Table show once again that the registration framework successfully optimized all the (dis)similarity measures ($p$<0.001) when the (dis)similarity measure values obtained before and after registration are compared. When the MSE is used as the dissimilarity measure, the increase of the degree of freedom of the geometric transformations brings about a significant ($p$<0.001) improvement in the dissimilarity measures.

The geometric transformations attained using different (dis)similarity measures on non-rigid registration were significantly divergent in some cases (Figure 3). This leads one to the following important conclusion: contrary to that has been verified in terms of intra-subject rigid registration, as far as inter-subject non-rigid registration is concerned, different (dis)similarity measures may lead to discrepant geometric transformations. The non-linear registration obtained by minimizing the MSE may produce more accentuated deformations than those obtained by optimizing the XOR or MI (Figure 3), which have been found to increase the processing time (Table 4). Figure 3 shows that in a number of cases of inter-subject non-linear registration, in which the MSE was optimized and bilinear interpolation was used, the deformation caused seems to be exaggerated. In such cases, the deformation is caused by the fact that there are regions in the template image that are not represented in the source image. However, the proposed framework attempted to create those regions so as to increase the image similarity. By using bicubic interpolation during the optimization process, the deformations were always found to be inferior or equal to those obtained when using bilinear interpolation.

Table 4 shows that minor variations occurred in the values of XOR and MI when the geometric transformation was modeled by a polynomial of the $2^{nd}$, $3^{rd}$ or $4^{th}$ degree. This Table also leads one to detect an unexpected and rather surprising fact: by minimizing the MSE when using polynomial geometric transformation of

the 3rd or 4th degree, the average MI values obtained are greater than the values obtained by directly maximizing the MI. We believe that this is because the MSE is more sensitive to the geometric transformation than the MI. Thus, some geometric transformations can lead to divergent MSE values whilst maintaining the MI value. In these cases, if the goal is to maximize the MI, then the optimization method could immediately be terminated as no changes will be obtained.

As far as inter-subject non-linear registration is concerned, particular attention should be paid when the MSE is minimized due to the possibility of major image deformations. Another important conclusion is that in the case of low resolution input images, such as those used in the experimental evaluation, the type of image interpolation has a significant effect on the geometric transformation obtained in the case of non-linear registration.

The optimization of the $MSE^{*}$ brought about some inappropriate image deformations in terms of non-linear inter-subject registration. Thus, this image dissimilarity measure should not be used on this particular kind of registration.

After matching the contour points obtained in the contour-based registration method, the estimation of the polynomial (of the 2nd or higher degree) geometric transformation that optimally overlaps the contours can be made. However, this non-linear geometric transformation should not be considered as the initial solution to use in the final optimization step of the framework, since there is no guarantee that it is a one-to-one function.

The convergence of the Powell's method to the optimal value of the (dis)similarity measures used is not guaranteed, mainly for XOR and MI. Nevertheless, a good initial guess for the geometric transformation that are the transformations attained using the contour-based and cross-correlation-based registration methods, guarantees that, if the global optimal value is not achieved, a local optimum very close to it is reached.

The Powell's method can be very time consuming; however, a good initial guess also guarantees that this method converges in a reduced number of iterations. Besides this, since the images considered are of low resolution, the time required in the image resampling and (dis)similarity measure calculations is always exceptionally low.

An approach frequently used to increase the likelihood of registration methods reaching the global maximum, or minimum, is based on the smoothing of the input images. However, this solution was confirmed to be inappropriate in the case of low resolution images as the preliminary tests conducted confirmed. In fact, in terms of low resolution images, the errors introduced by the smoothing process can have a considerable negative impact on the final results.
The main conclusion of the experimental evaluation which has been carried out is that the proposed registration framework is very accurate and fast for linear registration, i.e. rigid, similarity, affine and projective transformations, mainly when the MSE is used as the dissimilarity measure. Additionally, it is robust to data with noise and extremely versatile. Therefore, the framework allows both researchers and specialists in the medical field to choose different types of geometric transformations, distinct image (dis)similarity measures and different image interpolation methods, in accordance with the practical application in question, in order to attain reliable and efficient registration of pedobarographic image data.

## Acknowledgements

This work was partially done under the scope of the following research projects “Methodologies to Analyze Organs from Complex Medical Images – Applications to the Female Pelvic Cavity”, “Cardiovascular Imaging Modeling and Simulation - SIMCARD” and “Aberrant Crypt Foci and Human Colorectal Polyps: Mathematical Modelling and Endoscopic Image Processing”, with the references PTDC/EEA-CRO/103320/2008, UTAustin/CA/0047/2008 and UTAustin/MAT/0009/2008, respectively, financially supported by FCT - Fundação para a Ciência e a Tecnologia in Portugal.
The first author would like to acknowledge his PhD grant from Fundação Calouste Gulbenkian in Portugal.
The authors are particularly grateful to Dr Todd C. Pataky for providing the pedobarographic data set used in the experiments presented.

## References

[1] Actis R, Ventura L, Lott D, Smith K, Commean P, Hastings M, Mueller M (2008) Multi-plug insole design to reduce peak plantar pressure on the diabetic foot during walking. Med Biol Eng Comput 46:363-371

[2] Actis R, Ventura L, Smith K, Commean P, Lott D, Pilgram T, Mueller M (2006) Numerical simulation of the plantar pressure distribution in the diabetic foot during the push-off stance. Med Biol Eng Comput 44:653-663
[3] Bastos L, Tavares JMRS (2004) Improvement of modal matching image objects in dynamic pedobarography using optimization techniques. Lecture Notes in Computer Science 3179/2004. Springer, Berlin:39-50
[4] Collignon A, Maes F, Vandermeulen D, Marchal G, Suetens P (1997) Multimodality medical image registration by maximization of mutual information. IEEE Trans Med Imaging 16(2):187-198
[5] Emborg J, Spaich E, Andersen O (2009) Withdrawal reflexes examined during human gait by ground reaction forces: site and gait phase dependency. Med Biol Eng Comput 47:29-39
[6] Fradet L, Siegel J, Dahl M, Alimusaj M, Wolf S (2009) Spatial synchronization of an insole pressure distribution system with a 3D motion analysis system for center of pressure measurements. Med Biol Eng Comput 47:85-92
[7] Harrison AJ, Hillard PJ (2000) A moment-based technique for the automatic spatial alignment of plantar pressure data. Proceedings of the Institute of Mechanical Engineers, Part H: J Eng Medicine 214(3):257-264
[8] Keijsers N, Stolwijk N, Nienhuis B, Duysens J (2009) A new method to normalize plantar pressure measurements for foot size and foot progression angle. J Biomec 42:87-90
[9] Mattes D, Haynor D, Vesselle H, Lewellen T, Eubank W (2003) PET-CT image registration in the chest using free-form deformations. IEEE Trans Med Imaging 22(1):120-128
[10] Oliveira F, Tavares JMRS (2008) Algorithm of dynamic programming for optimization of the global matching between two contours defined by ordered points. Comput Modeling Eng Sci 31(1):1-11
[11] Oliveira F, Tavares JMRS (2009) Matching contours in images through the use of curvature, distance to centroid and global optimization with order-preserving constraint. Comput Modeling Eng Sci 43(1):91-110
[12] Oliveira F, Tavares JMRS, Pataky T (2009) Rapid pedobarographic image registration based on contour curvature and optimization. J Biomec 42(15):2620-2623
[13] Oliveira F, Tavares JMRS, Pataky T (2010) Registration of pedobarographic image data in the frequency domain. Comput Methods Biomec Biomed Eng, DOI: 10.1080/10255840903573020 (in press)
[14] Pataky T, Caravaggi P, Savage R, Parker D, Goulermas J, Sellers W, Crompton R (2008) New insights into the plantar pressure correlates of walking speed using pedobarographic statistical parametric mapping. J Biomec 41(9):1987-1994
[15] Pataky T, Goulermas J (2008) Pedobarographic statistical parametric mapping: a pixel-level approach to foot pressure image analysis. J Biomec 41(10):2136-2143
[16] Pataky T, Goulermas J, Crompton R (2008) A comparison of seven methods of within-subjects rigid-body pedobarographic image registration. J Biomec 41(14):3085-3089

[17] Pinho R, Tavares JMRS (2004) Dynamic pedobarography transitional objects by Lagrange's equation with FEM, modal matching and optimization techniques. Lecture Notes in Computer Science 3212/2004. Springer, Berlin, 92-99
[18] Press W, Teukolsky S, Vetterling W, Flannery B (2002) Numerical Recipes in C: the art of scientific computing, 2nd edition. Cambridge University Press, USA
[19] Rosenbaum D, Becker H (1997) Plantar pressure distribution measurements. Technical background and clinical applications. Foot and Ankle Surg 3(1):1-14
[20] Thévenaz P, Blu T, Unser M (2000) Interpolation revisited. IEEE Trans Med Imaging 19(7):739-758
[21] Viola P, Wells W (1997) Alignment by maximization of mutual information. Int J Comput Vis 24(2):137-154

**FIGURE CAPTIONS**

**Figure 1** Example of the registration of two pedobarographic images with noise using the framework developed. From left to the right: template image, source image, overlapped template and source images prior to registration, overlapped template and source images following registration, image differences between the template and source images after registration (To facilitate the visualization, the overlapped images were smoothed and binarized after the registration process)

**Figure 2** Spatial warping considered in the simulation of inter-subject registration: original image (on the left) and transformed image (on the right)

**Figure 3** Examples of image transformation obtained through the optimization of XOR, MSE and MI and the use of bilinear interpolation for rigid, projective and polynomial of the $2^{nd}$ degree geometric transformations

**Figure 4** Examples of image geometric deformations involving a $4^{th}$ degree polynomial transformation obtained by minimizing the MSE. From left to the right: template image, source image, transformed source image obtained through the use of bilinear interpolation, transformed source image obtained by using bicubic interpolation

## TABLE CAPTIONS

**Table 1** Comparison of the accuracy between the reference methods and the framework presented using XOR and $MSE^*$ as the dissimilarity measure for intra-subject rigid registration

**Table 2** Comparison among the residual errors obtained by the contour-based method, cross-correlation-based method and the framework presented, considering a known rigid geometric transformation

**Table 3** Comparison among the residual errors and (dis)similarity measures obtained considering a known warp geometric transformation and using the contour-based method, cross-correlation-based method and the framework presented

**Table 4** Average values obtained by the proposed framework using XOR, MSE and MI as the image (dis)similarity measure for inter-subjects registration (The initial registration was computed using the cross-correlation-based method)

**FIGURES**

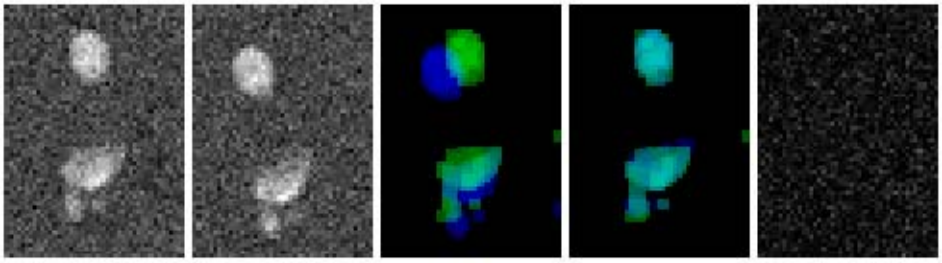

**Figure 1**

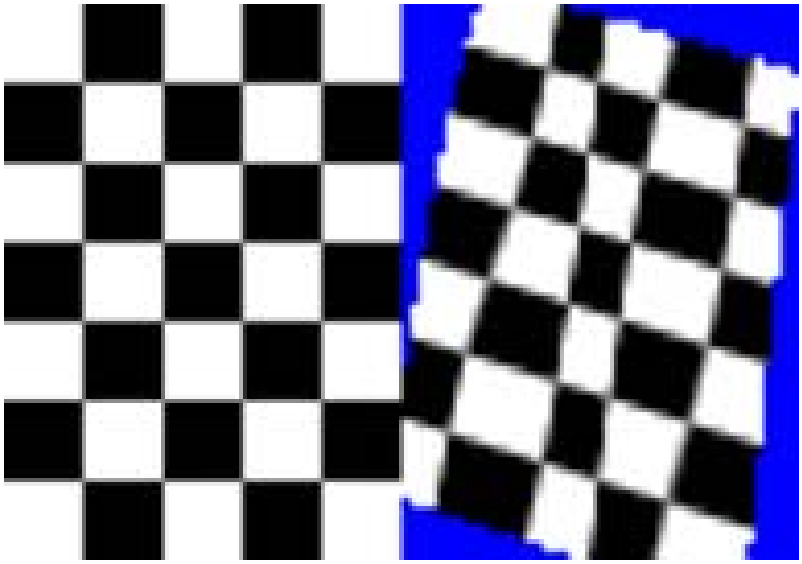

**Figure 2**

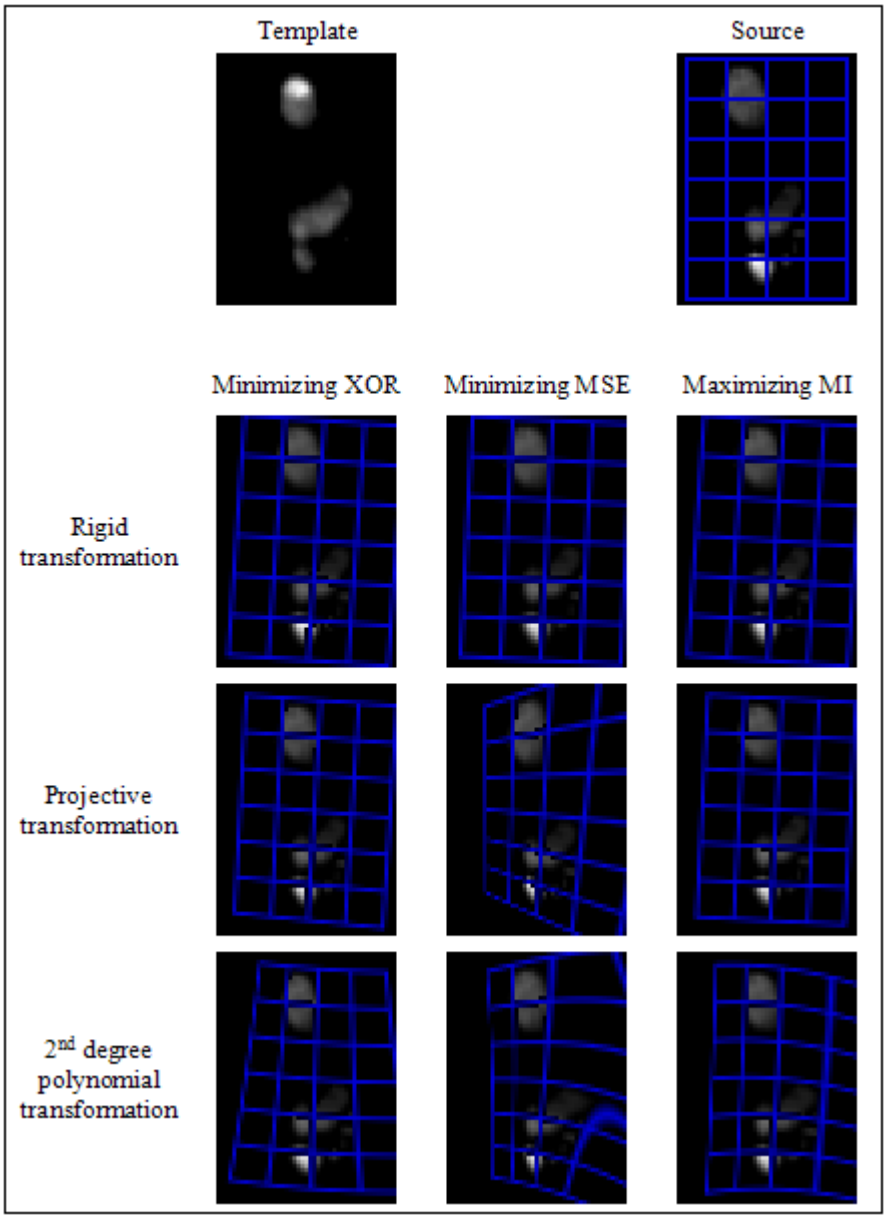


**Figure 3**

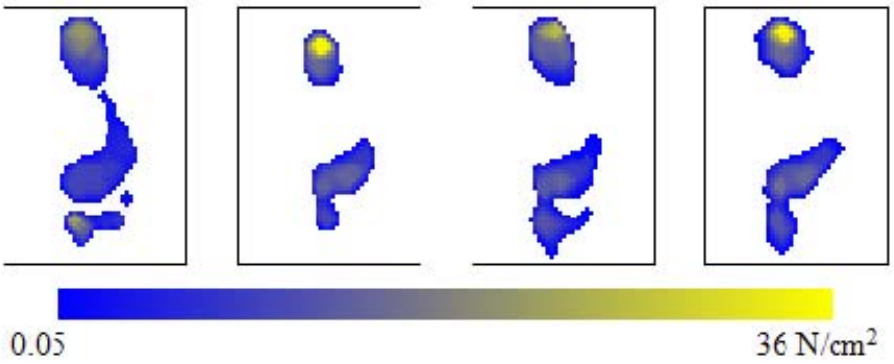


**Figure 4**

## TABLES

**Table 1**

| **Method** | **XOR [%]** | **Time [s]** | **MSE* [(N/cm$^2$)$^2$]** | **Time [s]** |
|---|---|---|---|---|
| Min(XOR) and Min(MSE*) methods based on evolutionary algorithms[1] [16] | 11.60 | 9.00 | 3.98 | 9.01 |
| Contour-based method with the pseudo optimization method [12] | 11.09 | 0.05 | 4.51 | 0.05 |
| Cross-correlation-based method [13] | 12.33 | 0.03 | 4.06 | 0.03 |
| Framework: Contour-based method (as in [12]) followed by the optimization based on Powell's method | 10.82 | 0.05 | 3.98 | 0.05 |
| Framework: Contour-based[2] method followed by the optimization based on Powell's method | 11.75 | 0.05 | 3.98 | 0.05 |
| Framework: Cross-correlation-based method followed by the optimization based on Powell's method | 11.70 | 0.07 | 3.98 | 0.07 |

[1]Min(XOR) and Min(MSE*) algorithms were implemented in MatLab.

[2]The initial geometric transformation was estimated using the least-squares technique after the contour matching.

**Table 2**

| | **Residual errors [pixels]** | | | |
|---|---|---|---|---|
| **Method(s)** | minXOR | minMSE | minMSE* | maxMI |
| Contour-based method | mean: 0.30 max: 0.60 | | | |
| Framework: Contour-based method followed by the optimization based on Powell's method | mean: 0.054<br>max: 0.28 | mean: $7.8\times10^{-6}$<br>max: $2.1\times10^{-5}$ | mean: $7.8\times10^{-6}$<br>max: $2.1\times10^{-5}$ | mean: $7.4\times10^{-3}$<br>max: 0.034 |
| Cross-correlation-based method | mean: 0.041 max: 0.088 | | | |
| Framework: Cross-correlation-based method followed by the optimization based on Powell's method | mean: 0.024<br>max: 0.075 | mean: $7.8\times10^{-6}$<br>max: $2.1\times10^{-5}$ | mean: $7.8\times10^{-6}$<br>max: $2.1\times10^{-5}$ | mean: $4.3\times10^{-3}$<br>max: 0.015 |
| | **Residual errors [pixels]** (after adding Gaussian noise) | | | |
| Contour-based method | mean: 0.36 max: 0.84 | | | |
| Framework: Contour-based method followed by the optimization based on Powell's method | XOR was not defined for this kind of noise | mean: 0.10<br>max: 0.34 | mean: 0.12<br>max: 0.50 | mean: 0.21<br>max: 0.69 |
| Cross-correlation-based method | mean: 0.14 max: 0.41 | | | |
| Framework: Cross-correlation-based method followed by the optimization based on Powell's method | XOR was not defined for this kind of noise | mean: 0.11<br>max: 0.33 | mean: 0.11<br>max: 0.42 | mean: 0.13<br>max: 0.31 |

**Table 3**

| | **Contour-based method** | **Cross-correlation-based method** | **Framework: Cross-correlation-based method followed by Powell's method** | | | | | | | |
|---|---|---|---|---|---|---|---|---|---|---|
| | | | minXOR | | minMSE | | minMSE* | | maxMI | |
| **Transformation** | RE | RE | XOR [%] | RE [pixel] | MSE [$(N/cm^2)^2$] | RE [pixel] | MSE* [$(N/cm^2)^2$] | RE [pixel] | MI | RE [pixel] |
| Rigid | 2.04 | 1.90 | 18.0 | 2.12 | 3.04 | 2.05 | 15.3 | 2.04 | 0.375 | 2.13 |
| Similarity | 1.88 | 1.79 | 14.0 | 1.87 | 1.54 | 1.86 | 8.66 | 1.85 | 0.393 | 1.87 |
| Affine | - | - | 7.58 | 1.12 | 0.34 | 0.91 | 2.25 | 0.91 | 0.433 | 1.36 |
| Projective | - | - | 6.39 | 1.10 | 0.13 | 0.75 | 0.87 | 0.76 | 0.445 | 1.28 |
| Polynomial of the $2^{nd}$ degree | - | - | 6.17 | 1.19 | 0.046 | 0.94 | 0.34 | 0.95 | 0.445 | 1.34 |
| Polynomial of the $3^{rd}$ degree | - | - | 6.08 | 1.43 | 0.011 | 0.89 | 0.18 | 0.93 | 0.445 | 1.46 |
| Polynomial of the $4^{th}$ degree | - | - | 5.78 | 1.49 | 0.006 | 1.06 | 0.26 | 1.39 | 0.448 | 1.42 |

**Table 4**

| **Cross-correlation-based method followed by the optimization based on Powell's method** (using bilinear interpolation) | | | | | | | | | | | | |
|---|---|---|---|---|---|---|---|---|---|---|---|---|
| **Before registration** | XOR: 34.2 | | | | MSE: 11.0 | | | | MI: 2.50 | | | |
| | Minimizing XOR | | | | Minimizing MSE | | | | Maximizing MI | | | |
| **Transformation** | XOR [%] | MSE | MI ×10 | Time [s] | XOR | MSE | MI ×10 | Time [s] | XOR | MSE | MI ×10 | Time [s] |
| Rigid | 21.9 | 7.17 | 3.53 | 0.08 | 24.2 | 6.44 | 3.47 | 0.09 | 23.3 | 6.85 | 3.64 | 0.15 |
| Similarity | 17.3 | 4.72 | 4.01 | 0.11 | 19.9 | 3.98 | 4.22 | 0.12 | 19.7 | 4.16 | 4.30 | 0.18 |
| Affine | 15.6 | 4.58 | 4.01 | 0.15 | 20.0 | 3.78 | 4.23 | 0.24 | 19.6 | 4.20 | 4.35 | 0.27 |
| Projective | 15.3 | 4.54 | 4.03 | 0.25 | 19.0 | 3.57 | 4.32 | 1.07 | 19.6 | 4.17 | 4.37 | 0.39 |
| Polynomial of the 2nd degree | 14.7 | 4.47 | 4.07 | 0.34 | 19.9 | 3.38 | 4.39 | 1.95 | 19.5 | 4.13 | 4.41 | 0.59 |
| Polynomial of the 3rd degree | 14.2 | 4.50 | 4.05 | 0.64 | 19.0 | 2.79 | 4.54 | 7.60 | 19.4 | 4.11 | 4.42 | 1.02 |
| Polynomial of the 4th degree | 14.0 | 4.46 | 4.08 | 1.26 | 17.6 | 2.51 | 4.62 | 31.0 | 19.5 | 4.12 | 4.44 | 1.97 |
| **Cross-correlation-based method followed by the optimization based on Powell's method** (using bicubic interpolation) | | | | | | | | | | | | |
| Rigid | 24.2 | 7.20 | 3.39 | 0.36 | 26.7 | 6.63 | 3.35 | 0.62 | 25.8 | 7.01 | 3.53 | 0.48 |
| Similarity | 20.2 | 4.52 | 3.95 | 0.49 | 22.2 | 4.04 | 4.10 | 0.93 | 22.4 | 4.30 | 4.20 | 0.62 |
| Affine | 19.0 | 4.53 | 3.92 | 0.79 | 22.1 | 3.83 | 4.11 | 2.18 | 22.3 | 4.28 | 4.24 | 0.99 |
| Projective | 18.6 | 4.43 | 3.96 | 1.06 | 21.3 | 3.59 | 4.19 | 6.07 | 22.2 | 4.28 | 4.28 | 1.45 |
| Polynomial of the 2nd degree | 18.1 | 4.34 | 4.02 | 1.85 | 22.2 | 3.39 | 4.28 | 11.4 | 22.3 | 4.22 | 4.31 | 2.05 |
| Polynomial of the 3rd degree | 17.7 | 4.35 | 4.00 | 3.10 | 20.9 | 2.77 | 4.45 | 42.0 | 22.3 | 4.19 | 4.34 | 3.20 |
| Polynomial of the 4th degree | 17.6 | 4.35 | 4.00 | 4.78 | 19.8 | 2.54 | 4.51 | 112 | 22.4 | 4.19 | 4.35 | 5.83 |